1 Biomineral repair of Abalone shell apertures

2 Maggie Cusack[1]*, DuJiao Guo[1], Peter Chung[1] and Nicholas A. Kamenos[1].

3 School of Geographical & Earth Sciences, University of Glasgow, Glasgow, G12 8QQ, UK.

4 *Maggie.Cusack@glasgow.ac.uk

5 Tel: 0141 330 5491/4224

6 Fax: 0141 330 4817

7

8

Abstract

The shell of the gastropod mollusc, abalone, is comprised of nacre with an outer prismatic layer that is composed of either calcite or aragonite or both, depending on the species. A striking characteristic of the abalone shell is the row of apertures along the dorsal margin. As the organism and shell grow, new apertures are formed and the preceding ones are filled in. Detailed investigations, using electron backscatter diffraction, of the infill in three species of abalone: *Haliotis asinina*, *Haliotis gigantea* and *Haliotis rufescens* reveals that, like the shell, the infill is composed mainly of nacre with an outer prismatic layer. The infill prismatic layer has identical mineralogy as the original shell prismatic layer. In *H. asinina* and *H. gigantea*, the prismatic layer of the shell and infill are made of aragonite while in *H. rufescens* both are composed of calcite. Abalone builds the infill material with the same high level of biological control, replicating the structure, mineralogy and crystallographic orientation as for the shell. The infill of abalone apertures presents us with insight into what is, effectively, shell repair.

Keywords: Abalone, aperture, shell repair, calcite, aragonite, EBSD

1. Introduction

As a model organism for biomineral research, the gastropod mollusc, abalone, has provided insights into many aspects of biomineralisation including gene expression (Degnan and Morse, 1995; Jackson et al., 2006; Jackson et al., 2010) and the role of specific organic components in shell formation (Bedouet et al., 2012; Falini et al., 2011; Jolly et al., 2004; Le Roy et al., 2012; Mann et al., 2007; Mann et al., 2000; Marie et al., 2010; Shen et al., 1997; Weiss et al., 2001; Weiss et al., 2000). Since nacre is the major component of the abalone shell, the attractive material properties of nacre, being light yet strong and crack-resistant (Jackson et al., 1988; Jackson et al., 1989; Jackson et al., 1990), accounts for the use of abalone shells as model systems for the study of the material properties of nacre e.g. (Chen et al., 2012; Espinosa et al., 2011; Lin and Meyers, 2009; Meyers et al., 2008). While nacre accounts for most of the abalone shell, the outermost layer is prismatic and the structure and crystallography of these two layers has also been investigated (Auzoux-Bordenave et al., 2010; Coppersmith et al., 2009; DiMasi and Sarikaya, 2004; Gilbert et al., 2008; Gries et al., 2009; Metzler et al., 2008).

A striking feature of abalone shell: the row of apertures along the dorsal margin (Figure 1) provides us with another potential insight into the diversity of biomineralisation. As the growing shell is formed new apertures are fabricated in a regular manner along the longitudinal growth margin while the preceding apertures are simultaneously filled in. This is a very interesting biomineralisation scenario since, not only is it creating a perfect hole during shell fabrication (to expel waste material) and for chemotaxis, but also manages a biomineral infill program, or, repair mechanism. The obvious question arises: is the formation of the infill as well controlled as the original shell formation (biologically controlled) or simply a rough plugging (inorganically) of a gap? This study examines the

nacre and prismatic layer of the shell and infill of three species of abalone in terms of mineralogy and crystallographic orientation in order to learn more about the aperture infill and to determine the extent to which it mimics the original and surrounding shell.

2. Materials and methods

2.1. Abalone specimens

Three species of abalone were considered: *Haliotis asinina*, *Haliotis gigantea* and *Haliotis rufescens*. Three adult specimens of each species were included in this study. Shells of *H. asinina* Linnaeus, 1758 from Australia (41°-10.5° S, 113°-153.5° E) were kindly provided by Professor Jackson and Professor Degnan. *H. gigantea* Gmelin, 1791 from Japan (31°-46° N, 130°-145.5° E) were kindly provided by Professor Endo (University of Tokyo). *H. rufescens* Swainson, 1822 from North America (25°-49° N, 125°-73° W) were kindly donated by Professor Taylor and Dr Claverie (University of California). Examples of the shells of these three species are presented in Figure 1.

2.2. Scanning electron microscopy including electron backscatter diffraction

Shell and infill microstructure and crystallography are analysed through Scanning Electron Microscopy (SEM) and Electron Backscatter Diffraction (EBSD) respectively. SEM imaging and EBSD analyses were carried out on the Quanta 200 from FEI in the Imaging, Spectroscopy and Analysis Centre (ISAAC) at the School of Geographical and Earth Sciences of the University of Glasgow. For SEM imaging, fractured shell sections were fixed to SEM stubs and gold-coated. For measurements of nacreous and prismatic layers, polished sections were carbon-coated and measurements made on secondary electron images. For

EBSD, shells were cut slowly under running water using an Isomet 5000 precision cutter from Buehler. Sections through the shells and through infilled apertures were embedded in resin and ground and polished through a sequence following a well-established method (Cusack et al., 2008; Perez-Huerta and Cusack, 2009). In summary, sections are ground using the following grit papers for 3 min each: P180 (82 µm), P320 (46 µm), P800 (21 µm), P1200 (15 µm) and P2500 (8 µm) and then P4000 (<5 µm) for 5 min. Followng grinding, polishing stages use alpha aluminium oxide at 1 µm and then 0.3 µm and finally a 5 min polish using 0.06 µm colloidal silica. Polished blocks are then coated with a thin layer of carbon (2.5nm). Polished, counted samples are mounted into SEM chamber, tilted to 70º and then EBSD data gathered using an accelerating voltage of 20 kV, working distance of 10 mm, aperture of 50 nm and step size of 0.2 µm. All data points below a confidence index [CI] of 0.1 were removed and data analyzed using OIM 6 software from EDAX-TSL. Data are then presented as maps of diffraction intensity, phase or crystallographic orientation.

3. Results

3.1. Shell structure

The shell of abalone is composed mainly of nacre with an outer prismatic layer (Figure 2). The prismatic layer thickness is different in the three species studied and bears no relationship to the overall shell thickness (Figure 3). While *H. gigantea* is the thickest shell in this study, the prismatic layer was no thicker than that of *H. asinina*. *H. rufescens* has a relatively thin shell where the prismatic layer accounts for almost 50% of the shell thickness (Figure 3).

Dauphin et al., (1989) used shell chemistry to determine the mineralogy of the prismatic shell layer in ten species of abalone using higher relative abundance of Sr, Na and

K to indicate aragonite and higher concentrations of Mg and Mn to indicate calcite. Of their survey, two species, including *H. asinina* have a prismatic layer composed of aragonite only, two others, including *H. rufescens*, have a prismatic layer of calcite only and the prismatic layer of the other six species have both calcite and aragonite. Dauphin et al., (1989) point out that concentrations of these elements that signature the calcium carbonate polymorphs, are close to detection limit. In this study, electron backscatter diffraction (EBSD) is used to compare the prismatic layer of shell and infill since EBSD readily distinguishes between calcite and aragonite and provides insight into crystallographic orientation in context.

3.2. Mineralogy of prismatic layer of the shell

EBSD analyses of the shell indicate that the prismatic layer of *H. asinina* and *H. gigantea* consists of aragonite while that of *H. rufescens* is comprised of calcite (Figure 4). The prismatic layer of *H. asinina* and *H. gigantea* are similar, consisting of fine-grained aragonite structures. In contrast, the calcite of the shell prisms of *H. rufescens* consists of large crystals, often well over 100 µm.

3.3. Mineralogy of prismatic layer of the aperture infill

Apertures are infilled in the same direction as shell growth (Figure 5). The banding of the infill (Figure 5B) suggests a pulsed process of regular increments. EBSD analyses of the aperture infill indicate that the prismatic layer of *H. asinina* and *H. gigantea* consists of aragonite while that of *H. rufescens* is comprised of calcite (Figure 6). The similarity between shell and infill prismatic layers is clear with *H. asinina* and *H. gigantea* having small aragonite crystals in both and *H. rufescens* having large calcite crystals in the prismatic layer

of the shell and aperture infill. The material in the outermost region of the prismatic layer of shell (Figure 4I) and aperture infill (Figure 6I) of *H. rufescens* is very fine-grained suggesting that the material in this outermost region is either too fine or too porous to diffract, in contrast to the large calcite crystals which diffract well (Figures 4I, 6I).

3.4. Interface between aperture in-fill and shell

The image in Figure 7 is that of a completely flat surface and the apparent raised aperture rim is an optical illusion. The surface of *H. asinina* shell has been polished in the area of a completely filled-in aperture, in a downward direction from the outside towards the interior. Thus Figure 7 depicts a bird's eye view of the interior of an aperture that has been filled in completely and the interface between the infill and the shell. The interface between the infill and shell aperture is flawless with no gaps or ragged edges apparent (Figure 7). The crystallographic orientation of the infill and shell is well constrained as depicted in Figure 7. The phase map in Figure 7B confirms the presence of aragonite only. The crystallographic orientation map (Figure 7C) with corresponding pole figure (Figure 7D) demonstrates the strict control on crystallographic orientation of the infill and shell which cannot be distinguished in terms of crystallographic orientation.

4. Discussion

In the three species of abalone studied here, there is no evidence that back-filling of shell apertures is a rough 'plugging-in' of a gap. Instead, exquisite biological control is exerted in all aspects with the aperture infill sharing the mineralogy, structure and crystallographic control with the shell in a species-specific manner. A wider study may be required before

concluding that this is a generality for abalone but there is nothing here to suggest that it may be otherwise.

There is active interest in understanding shell repair (Fleury et al., 2008; Kijima et al., 2011) by first of all, inducing damage e.g. by etching (Kijima et al., 2011) or drilling out a plug (Fleury et al., 2008) from the shell. Fleury et al (2008) drilled plugs of 7mm diameter about 0.5 – 1 cm from the shell edge of adult specimens of *H. tuberculata* and analysed the repaired plugs using scanning electron microscopy. In contrast to the developmental aperture infills that consist of outer prismatic and inner nacreous layers, these repaired holes were stratified with several microstructural types: spherulitic, thin prismatic, blocklike, sub-nacreous, nacreous and foliated-like microstructures. The prismatic and nacreous layers of developmental infills form generally continuous layers while the more numerous microstructures of the repaired holes tend to be discontinuous and more lenticular in occurrence. These differences in developmental and experimentally-induced infills suggest a more ad-hoc, yet effective, route to repair of holes beyond the usual developmental stages and processes.

Repair of natural environmental damage (Harper et al., 2012) is another aspect of interest. In the fossil record, it is important to be able to identify damage that occurred while the animal was alive and any repair that may have taken place. Such interest in shell damage in the fossil record includes calcium carbonate shells (Harper, 2003; Kroger, 2011) as well as calcium phosphate shells (Freeman and Miller, 2011). Although abalone apertures are not areas of true damage caused by accident or injury since the apertures are part of the shell development, nonetheless, the mechanism by which abalone fills in the apertures deserves further investigation to seek insight into how biomineral repair might be achieved. Viewing the shell exterior, it is clear that the aperture infill consists of a series of bands (Figure 5) of quite uniform thickness (about 20 μm), suggesting that the bands are emplaced in stages as

the aperture in-filling proceeds. These bands can sometimes be seen in cross–section (see Figure 6G to top right of EBSD area). Elucidating the mechanism by which these bands are emplaced will be key to understanding how abalone fills in shell apertures with such exquisite control.

Acknowledgements

Sincere thanks to Professor Bernie Degnan and Professor Daniel Jackson for providing *H. asinina*, Professor Kazuyoshi Endo for providing *H. gigantea* shells and Professor Taylor and Dr Claverie for making *H. rufescens* available for this study. DG gratefully acknowledges a Scholarship from the Chinese Scholarship Council (CSC). We thank the two anonymous reviewers for their very helpful comments. MC would like to take this opportunity to thank Steve Weiner for always asking the fundamental questions about biomineralisation.

Figure descriptions

Figure 1 Shells of three species of abalone: *H. asinina*, *H. gigantea* and *H. rufescens*.

Exterior (A, C, E) and interior (B, D, F) of shells of *H. asinina*, *H. gigantea* and *H. rufescens* respectively. Scale bars = 10, 5 and 5 mm respectively.

Figure 2 Prisms and nacre of *H. asinina* shell.

Secondary electron images of fractured shell section of *H. asinina* revealing (A) outer prismatic (P) layer and inner nacreous (N) layer with interface between the two layers

indicated by dashed white line. Higher magnification images of (B) prismatic layer and (C) nacreous layer. Scale bars = 200 µm, 50 µm and 2 µm respectively.

Figure 3 Thickness relationships of prismatic layer and the corresponding cross-section in *H. asinina, H. gigantea and H. rufescens* shells.

(A) The average (n = 24) thickness and standard deviation (S.D.) of cross-section shell and prismatic layer of individual shells of three species of abalone. (B) The average (n = 24) thickness of prismatic layer as a percentage of whole shell thickness and S.D.

Figure 4 Mineralogy of prismatic layer of *H. asinina, H. gigantea* and *H. rufescens shell.*

(A, D, G) Secondary electron images of polished sections of the prismatic region, (B, E, H) diffraction intensity maps and (C, F, I) phase maps of *H. asinina*, *H. gigantea* and *H. rufescens* respectively. Diffraction intensity maps (B, E, H) and phase maps (C, F, I) are shown corresponding to the blue box in the secondary electron images (A, D, G). Scale bar = 100, 50 and 100 µm for *H. asinina*, *H. gigantea* and *H. rufescens* respectively. In each case, section is from the mid region of the shell, parallel to the shell length, with shell exterior to the top of the image.

Figure 5 Half-filled aperture of *H. asinina*

(A) Secondary electron image of half-filled aperture of *H. asinina* with arrow indicating growth direction and coincident direction of in-fill growth. White box in A indicates area

presented in (B) at higher magnification to show the banding of the infill as the infill develops in stages. Scale bars = 500 µm and 100 µm for A and B respectively.

Figure 6 Mineralogy of aperture infill of *H. asinina, H. gigantea* and *H. rufescens shells*

(A, D, G) Secondary electron images of polished sections of aperture infill, (B, E, H) diffraction intensity maps and (C, F, I) phase maps of *H. asinina*, *H. gigantea* and *H. rufescens* respectively. Diffraction intensity maps (B, E, H) and phase maps (C, F, I) are shown corresponding to the blue box in the secondary electron images (A, D, G). Scale bar = (A) = 80 µm (B, C) = 35 µm, (D) = 200, (E, F) = 80 (G) = 1 mm (H, I) = 40 µm for *H. asinina*, *H. gigantea* and *H. rufescens* respectively. In each case sections were cut, perpendicular to growth direction, through infilled apertures with anterior margin towards right of image.

Figure 7. Mineralogy and crystallographic orientation of aperture infill and surrounding shell of *H. asinina.*

The surface of *H. asinina* shell has been polished in the area of a completely filled-in aperture, in a downward direction from the outside towards the interior. (A) Diffraction intensity map of aperture infill (left) and surrounding shell (right) of *H. asinina* polished top down. Scale bar = 70 µm. Dashed white line indicates interface of infill (left) and shell (right) with white arrow indicating direction of infill and shell growth. (B) Phase map of same area with aragonite in red (if calcite were present, it would be indicated in green). (C) Map of crystallographic orientation with corresponding pole figure (D). Colour in (C) and (D) correspond to colour key (E).

References

Auzoux-Bordenave, S., Badou, A., Gaume, B., Berland, S., Helleouet, M.N., *et al.*, 2010. Ultrastructure, chemistry and mineralogy of the growing shell of the European abalone Haliotis tuberculata. J Struct Biol 171, 277-290.

Bedouet, L., Marie, A., Berland, S., Marie, B., Auzoux-Bordenave, S., *et al.*, 2012. Proteomic Strategy for Identifying Mollusc Shell Proteins Using Mild Chemical Degradation and Trypsin Digestion of Insoluble Organic Shell Matrix: A Pilot Study on Haliotis tuberculata. Mar Biotechnol 14, 446-458.

Chen, B., Yin, D.G., Wang, J.G., Yuan, Q., Fan, J.H., 2012. Laminated microstructure and toughness mechanism of abalone shell, p. 133-135, in: M. Jan and S. Ezhilvalavan, Eds.), Advanced Structural and Functional Materials for Protection.

Coppersmith, S.N., Gilbert, P., Metzler, R.A., 2009. Theoretical characterization of a model of aragonite crystal orientation in red abalone nacre. Journal of Physics a-Mathematical and Theoretical 42.

Cusack, M., England, J., Parkinson, D., Dalbeck, P., Lee, M.L., *et al.*, 2008. Oxygen isotope composition, magnesium distribution and crystallography of *Terebratulina retusa*. Fossils & Strata 54, 259-267.

Dauphin, Y., Cuif, J.-P., Mutvei, H., Denis, A., 1989. Mineralogy, chemistry and ultrastructure of the external shell-layer in ten species of Haliotis with reference to *Haliotis tuberculata* (Mollusca: Archaeogastropoda). Bulletin of the Geological Institutions of the University of Uppsala 15, 7-37.

Degnan, B.M., Morse, D.E., 1995. Developmental and morphogenetic gene-regulation in *Haliotis rufescens* larvae at metamorphosis. Am Zool 53, 391-398.

DiMasi, E., Sarikaya, M., 2004. Synchrotron x-ray microbeam diffraction from abalone shell. J Mater Res 19, 1471-1476.

Espinosa, H.D., Juster, A.L., Latourte, F.J., Loh, O.Y., Gregoire, D., *et al.*, 2011. Tablet-level origin of toughening in abalone shells and translation to synthetic composite materials. Nature Communications 2.

Falini, G., Sartor, G., Fabbri, D., Vergni, P., Fermani, S., *et al.*, 2011. The interstitial crystal-nucleating sheet in molluscan Haliotis rufescens shell: A bio-polymeric composite. J Struct Biol 173, 128-137.

Fleury, C., Marin, F., Marie, B., Luquet, G., Thomas, J., *et al.*, 2008. Shell repair process in the green ormer Haliotis tuberculata: A histological and microstructural study. Tissue Cell 40, 207-218.

Freeman, R.L., Miller, J.F., 2011. FIRST REPORT OF A LARVAL SHELL REPAIR SCAR ON A LINGULATE BRACHIOPOD: EVIDENCE OF DUROPHAGOUS PREDATION IN THE CAMBRIAN PELAGIC REALM? J Paleontol 85, 695-702.

Gilbert, P., Metzler, R.A., Zhou, D., Scholl, A., Doran, A., *et al.*, 2008. Gradual Ordering in Red Abalone Nacre. J Am Chem Soc 130, 17519-17527.

Gries, K., Kroger, R., Kubel, C., Schowalter, M., Fritz, M., *et al.*, 2009. Correlation of the orientation of stacked aragonite platelets in nacre and their connection via mineral bridges. Ultramicroscopy 109, 230-236.

Harper, E.M., 2003. Assessing the importance of drilling predation over the Palaeozoic and Mesozoic. Palaeogeogr palaeocl 210, 185-198.

Harper, E.M., Clark, M.S., Hoffman, J.I., Philipp, E.E.R., Peck, L.S., *et al.*, 2012. Iceberg Scour and Shell Damage in the Antarctic Bivalve Laternula elliptica. PLoS One 7.

Jackson, A.P., Vincent, J.F.V., Turner, R.M., 1988. The Mechanical Design of Nacre. Proceedings of The Royal Society of London Series B-Biological Sciences 234, 415-440.

Jackson, A.P., Vincent, J.F.V., Turner, R.M., 1989. A Physical Model of Nacre. Composites Science And Technology 36, 255-266.

Jackson, A.P., Vincent, J.F.V., Turner, R.M., 1990. Comparison of Nacre with other Ceramic Composites. J Mater Sci 25, 3173-3178.

286 Jackson, D.J., McDougall, C., Green, K., Simpson, F., Worheide, G., *et al.*, 2006. A rapidly evolving
287 secretome builds and patterns a sea shell. BMC Biology 4.
288 Jackson, D.J., McDougall, C., Woodcroft, B., Moase, P., Rose, R.A., *et al.*, 2010. Parallel Evolution
289 of Nacre Building Gene Sets in Molluscs. Mol Biol Evol 27, 591-608.
290 Jolly, C., Berland, S., Milet, C., Borzeix, S., Lopez, E., *et al.*, 2004. Zonal localization of shell matrix
291 proteins in mantle of Haliotis tuberculata (Mollusca, Gastropoda). Mar Biotechnol 6, 541-
292 551.
293 Kijima, M., Oaki, Y., Imai, H., 2011. In Vitro Repair of a Biomineral with a Mesocrystal Structure.
294 Chem-Eur J 17, 2828-2832.
295 Kroger, B., 2011. Size matters - Analysis of shell repair scars in endocerid cephalopods. Fossil
296 Record 14, 109-118.
297 Le Roy, N., Marie, B., Gaume, B., Guichard, N., Delgado, S., *et al.*, 2012. Identification of Two
298 Carbonic Anhydrases in the Mantle of the European Abalone Haliotis tuberculata
299 (Gastropoda, Haliotidae): Phylogenetic Implications. Journal of Experimental Zoology Part
300 B-Molecular and Developmental Evolution 318B, 353-367.
301 Lin, A.Y.M., Meyers, M.A., 2009. Interfacial shear strength in abalone nacre. Journal of the
302 Mechanical Behavior of Biomedical Materials 2, 607-612.
303 Mann, K., Weiss, I.M., Andre, S., Gabius, H.-J., Fritz, M., 2000. The amino-acid sequence of the
304 abalone (Haliotis laevigata) nacre protein perlucin. Detection of a functional C-type lectin
305 domain with galactose/mannose specificity. Eur J Biochem 267, 5257-5264.
306 Mann, K., Siedler, F., Treccani, L., Heinemann, F., Fritz, M., 2007. Perlinhibin, a cysteine-, histidine-,
307 and arginine-rich miniprotein from abalone (Haliotis laevigata) nacre, inhibits in vitro
308 calcium carbonate crystallization. Biophys J 93, 1246-1254.
309 Marie, B., Marie, A., Jackson, D.J., Dubost, L., Degnan, B.M., *et al.*, 2010. Proteomic analysis of the
310 organic matrix of the abalone Haliotis asinina calcified shell. Proteome Science 8.
311 Metzler, R.A., Zhou, D., Abrecht, M., Chiou, J.W., Guo, J.H., *et al.*, 2008. Polarization-dependent
312 imaging contrast in abalone shells. Physical Review B 77.

313 Meyers, M.A., Lin, A.Y.M., Chen, P.Y., Muyco, J., 2008. Mechanical strength of abalone nacre: Role
314 of the soft organic layer. Journal of the Mechanical Behavior of Biomedical Materials 1, 76-
315 85.
316 Perez-Huerta, A., Cusack, M., 2009. Optimizing Electron Backscatter Diffraction of Carbonate
317 Biominerals-Resin Type and Carbon Coating. Microsc Microanal 15, 197-203.
318 Shen, X., Belcher, A.M., Hansma, P.K., Stucky, G.D., Morse, D.E., 1997. Molecular cloning and
319 characterization of Lustrin A, a matrix protein from shell and pearl nacre of *Haliotis*
320 *rufescens*. J Biol Chem 272, 32472-32481.
321 Weiss, I.M., Kaufmann, S., Mann, K., Fritz, M., 2000. Purification and characterization of Perlucin
322 and Perlustrin, two new proteins from the shell of the mollusc Haliotis laevigata. Biochem
323 Biophys Res Commun 267, 17-21.
324 Weiss, I.M., Gohring, W., Fritz, M., Mann, K., 2001. Perlustrin, a Haliotis laevigata (abalone) nacre
325 protein, is homologous to the insulin-like growth factor binding protein N-terminal module of
326 vertebrates. Biochem Biophys Res Commun 285, 244-249.
327
328

Figure

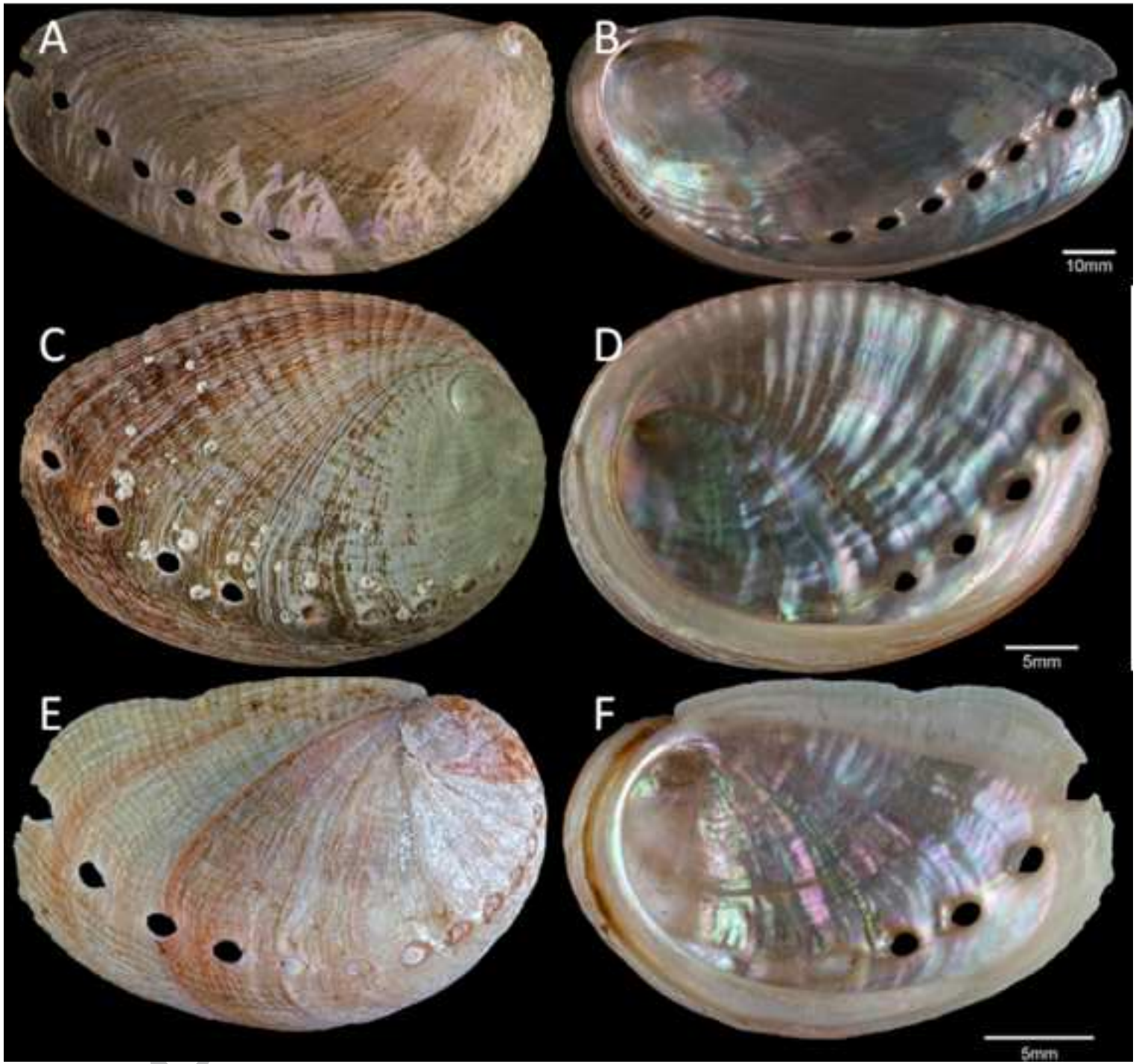

Figure

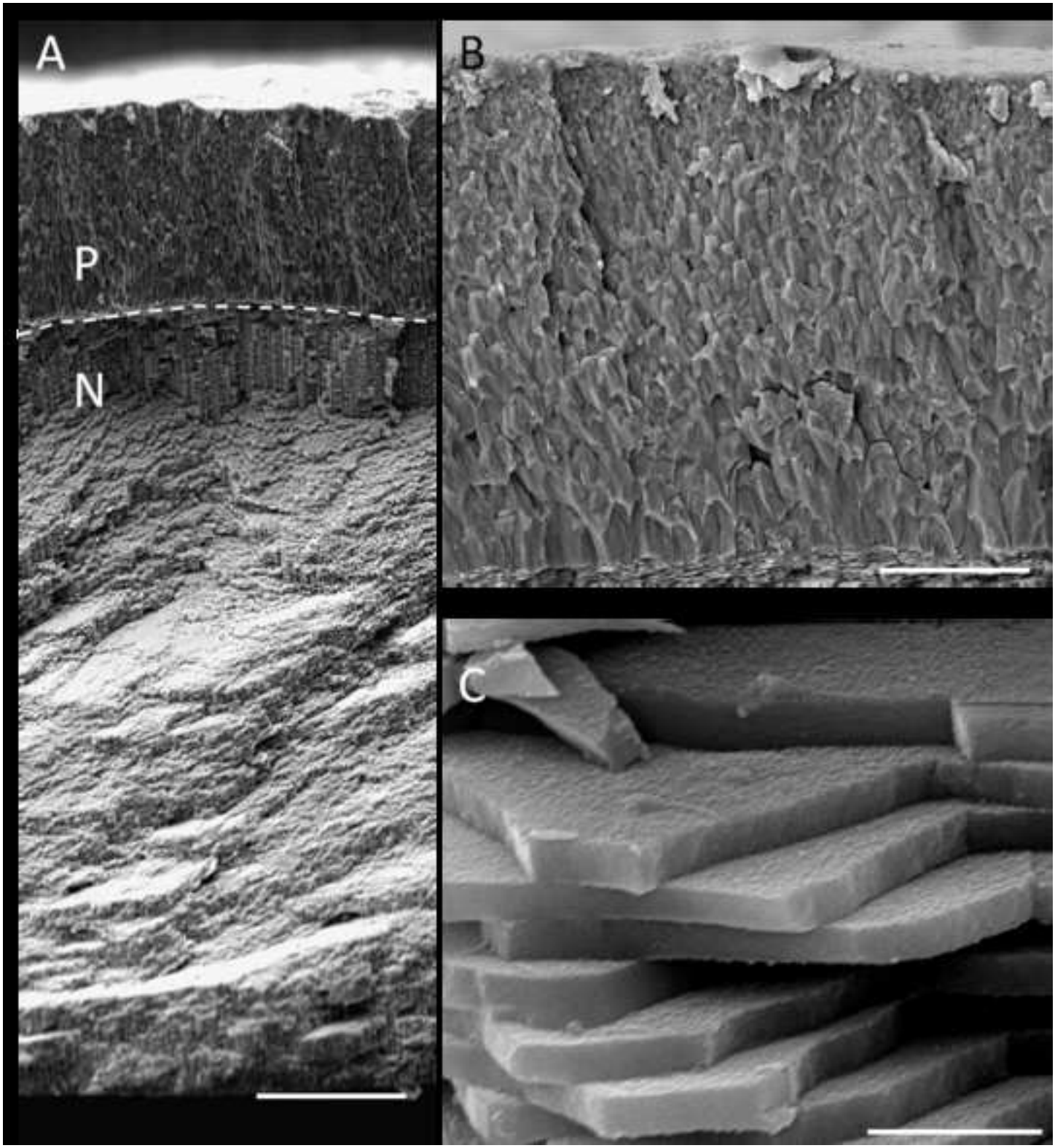

Figure

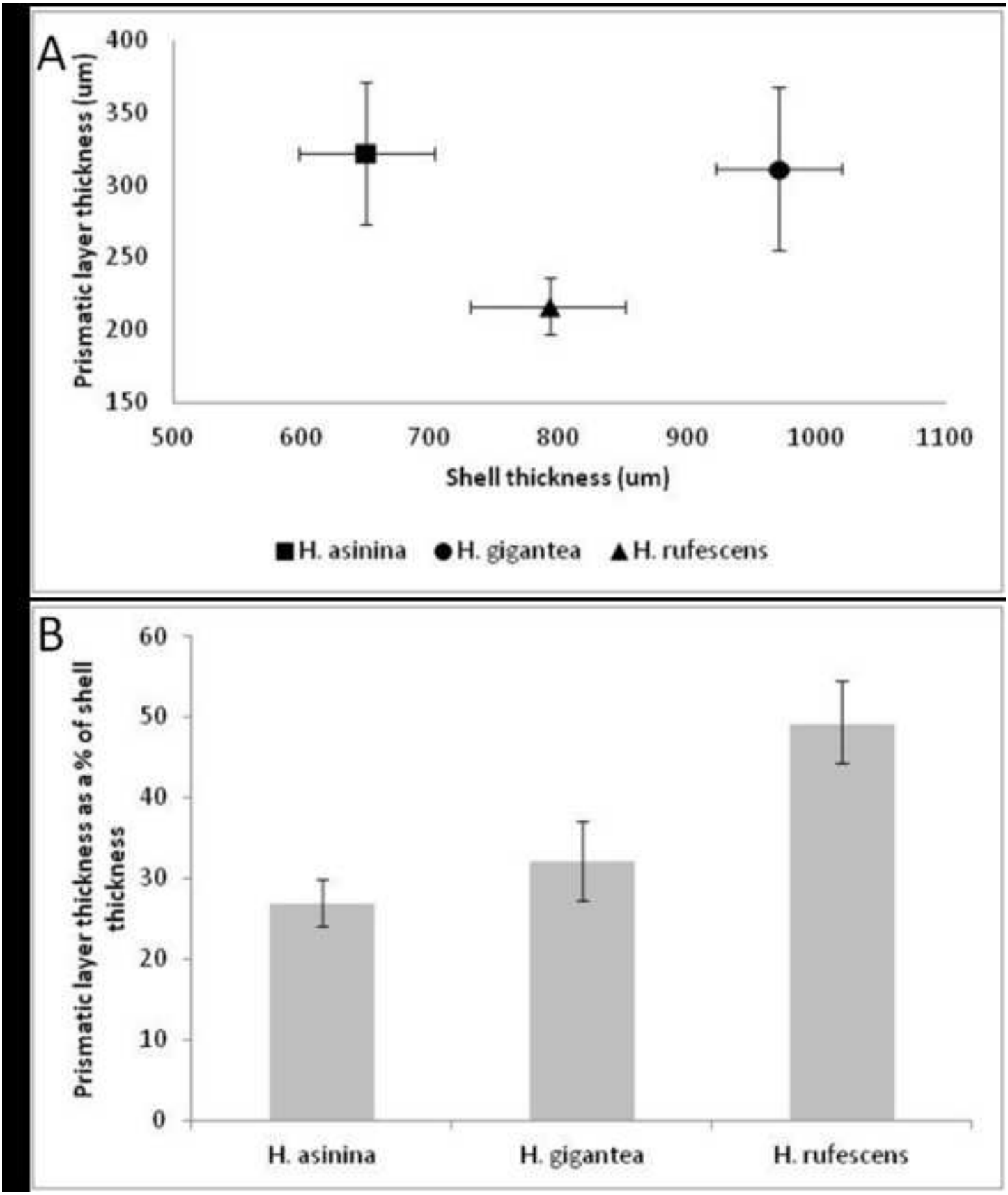

Figure

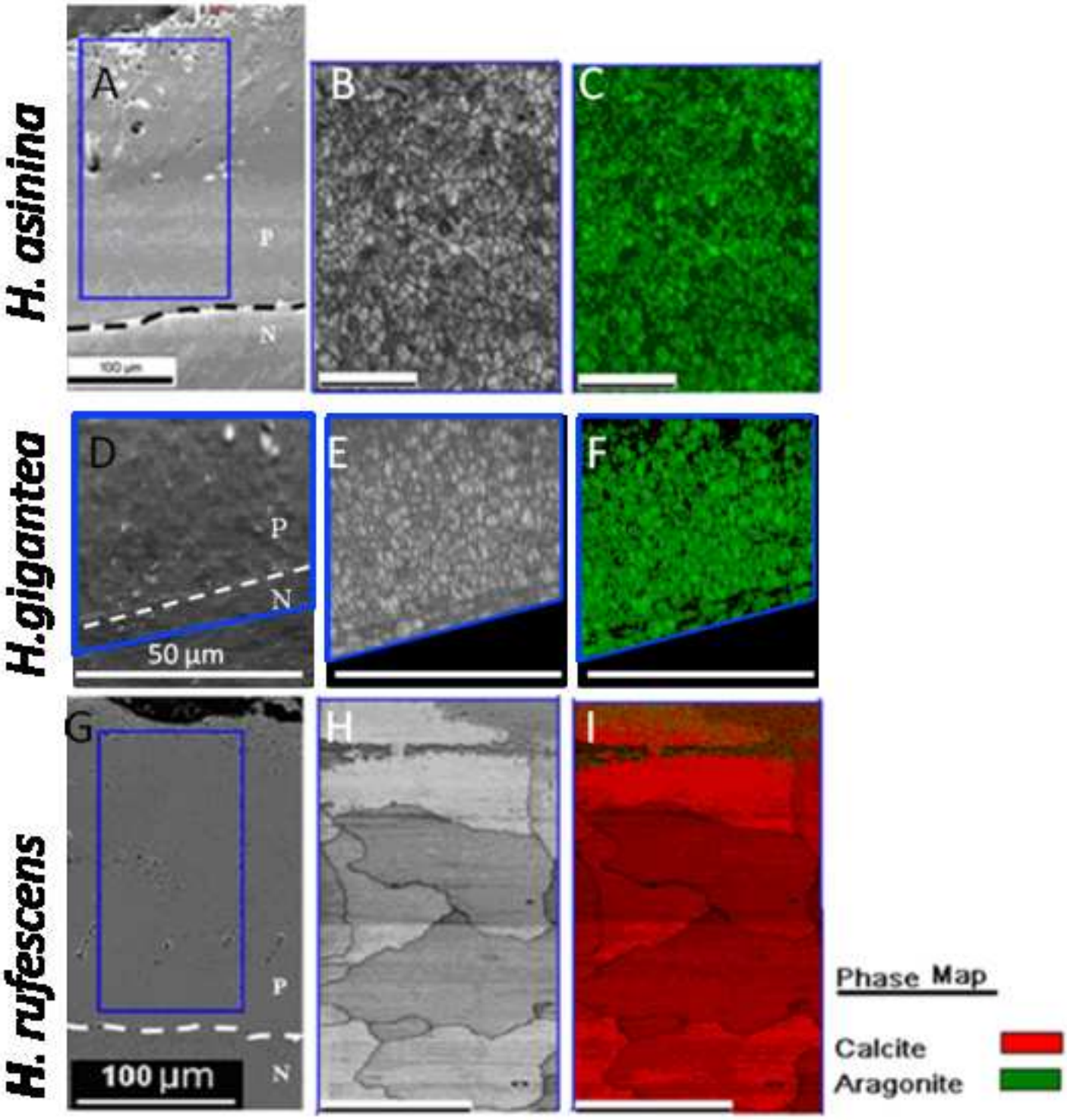

Figure

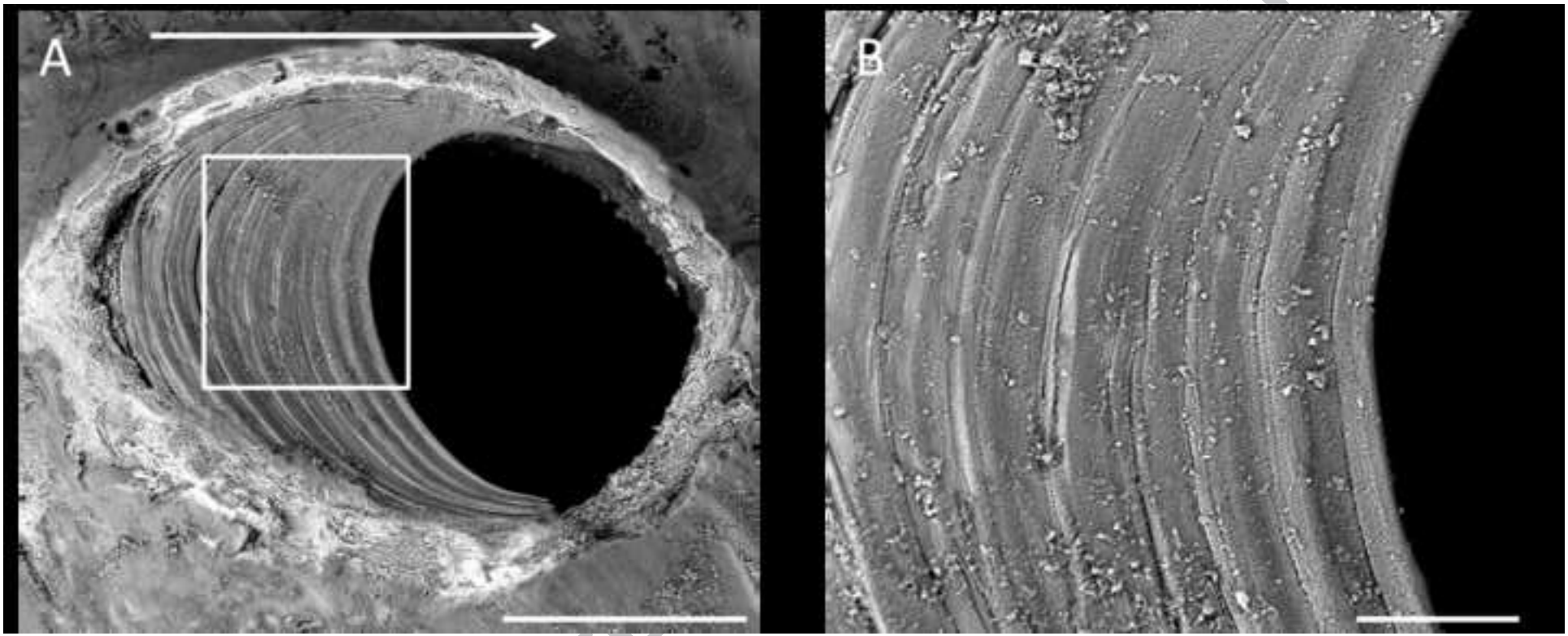

Figure

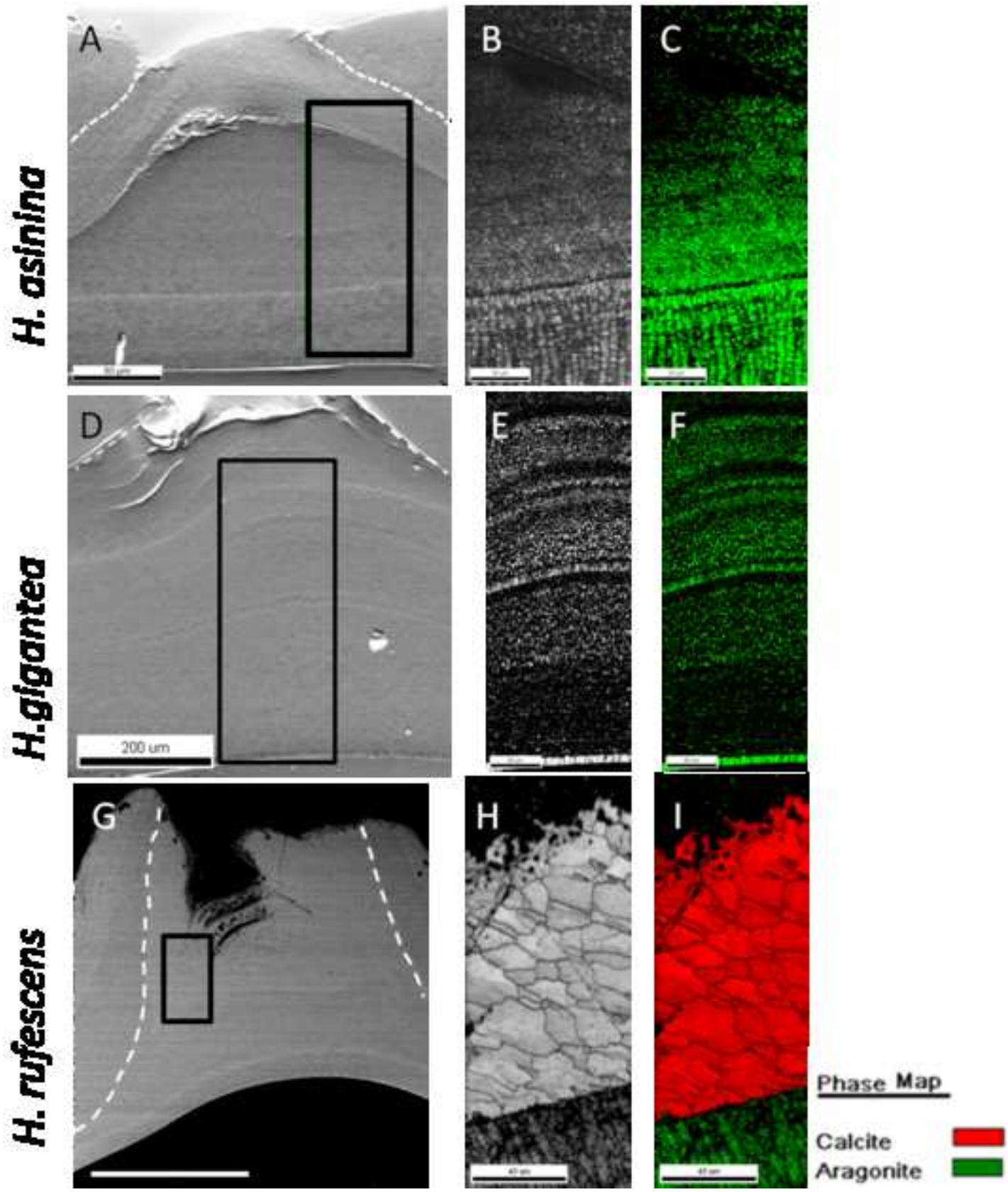

Figure